

Gamma-Ray Bursts via the Neutrino Emission from Heated Neutron Stars

Jay D. Salmonson¹ and James R. Wilson

Lawrence Livermore National Laboratory, Livermore, CA 94550

Grant J. Mathews

University of Notre Dame, Notre Dame, IN 46556

ABSTRACT

A model is proposed for gamma-ray bursts based upon a neutrino burst of $\sim 10^{52}$ ergs lasting a few seconds above a heated collapsing neutron star. This type of thermal neutrino burst is suggested by relativistic hydrodynamic studies of the compression, heating, and collapse of close binary neutron stars as they approach their last stable orbit, but may arise from other sources as well. We present a spherically symmetric hydrodynamic simulation of the formation and evolution of the pair plasma associated with such a neutrino burst. This pair plasma leads to the production of $\sim 10^{51} - 10^{52}$ ergs in γ -rays with spectral and temporal properties consistent with many observed gamma-ray bursts.

Subject headings: binaries: close — gamma rays: bursts — gamma rays: theory — stars: neutron

1. Introduction

Understanding the origin of gamma-ray bursts (GRBs) has been a perplexing problem since they were first detected almost three decades ago (Klebesadel et al. 1973). The fact that GRBs are distributed isotropically (Meegan et al. 1992) suggests a cosmological origin. Furthermore, arcminute burst locations from BeppoSax have revealed that at least some γ -ray bursts involve weak X-ray, optical, or radio transients, and are of cosmological origin (Groot et al. 1997). The Mg I absorption and [O II] emission lines along the line of sight from the GRB970508 optical transient, for example, indicate a redshift $Z \geq 0.835$ (Galama et al. 1997). The implied distance means that this burst must have released of order $\sim 10^{51}$ ergs in γ -rays on a time scale \sim seconds. This energy requirement has been rendered even more demanding by other events such as GRB971214 (Kulkarni et al. 1998) which appears to be centered on a galaxy at redshift 3.42. This implies that the energy of a 4π burst would have to be as much as 3×10^{53} ergs, comparable to the visible light output of $\sim 10^9$ galaxies.

¹e-mail: salmonson@llnl.gov

Based upon the accumulated evidence one can now conclude that the following four features probably characterize the source environment: 1) If the total burst energies are in the range of $10^{51} - 10^{52}$ ergs, then a beaming factor of 10 to 100 is necessary; 2) The multiple peak temporal structure of most bursts probably requires either multiple colliding shocks (Rees & Mészáros 1994; Kobayashi et al. 1998) or a single shock impinging upon a clumpy interstellar medium (Mészáros & Rees 1993; Dermer & Mitman 1999); 3) The observed afterglows imply some surrounding material on a scale of light hours; and 4) the presence of [O II] emission lines suggests that the bursts occur in a young, metal-enriched stellar population.

Some proposed sources for the production of GRBs include accretion onto supermassive black holes, AGN's, relativistic stellar collisions, hypernovae, and binary neutron star coalescence. Each of these possibilities, however, remain speculative until realistic models can be constructed for their evolution. In this paper we construct a model for GRBs produced by energetic neutrino emission from a heated neutron star. Our specific model for the emission derives from the relativistic compression and heating of neutron stars near their last stable orbit, however any scenario by which energetic neutrino emission above a neutron star can endure for several seconds (e.g. tidal heating, MHD induced heating, accretion shocks, etc) might also power the gamma-ray burst paradigm described herein.

Our model is as follows. A compressionally heated neutron star emits thermal neutrino pairs which, in turn, annihilate to produce a hot electron-positron pair plasma. We model the expansion of the plasma with a spherically symmetric relativistic hydrodynamics computer program. This simplification is justified at this stage of the calculations since the rotational velocity of the stars is about one third of the sound speed in the e^+e^- pair plasma. We then analyze and compare the contributions of photons from e^+e^- pair annihilation as well as from an external synchrotron shock as the plasma plows into the interstellar medium. We show that the characteristic features of GRBs, i.e. total energy, duration and gamma-ray spectrum, can be accounted for in the context of this model.

2. Compression in Close Neutron Star Binaries

It has been speculated for some time that inspiraling neutron stars could provide a power source for cosmological gamma-ray bursts. However, previous Newtonian and post Newtonian studies (Janka & Ruffert 1996; Ruffert & Janka 1998, 1999) of the final merger of two neutron stars have found that the neutrino emission time scales are so short that it would be difficult to drive a gamma-ray burst from this source. It is clear that a mechanism is required for extending the duration of energetic neutrino emission. A number of possibilities could be envisioned, for example, neutrino emission powered by accretion shocks, MHD or tidal interactions between the neutron stars, etc. The present study, however, has been primarily motivated by numerical studies of the strong field relativistic hydrodynamics of close neutron-star binaries in three spatial dimensions. These studies (Wilson & Mathews 1995; Wilson et al. 1996; Mathews & Wilson 1997; Mathews

et al. 1998; Mathews & Wilson 2000) suggest that neutron stars in a close binary can experience relativistic compression and heating over a period of seconds. During the compression phase released gravitational binding energy can be converted into internal energy. Subsequently, up to 10^{53} ergs in thermally produced neutrinos can be emitted before the stars collapse (Mathews & Wilson 1997, 2000). Here we briefly summarize the physical basis of this model and numerically explore its consequences for the development of an e^+e^- plasma and associated GRB.

In (Mathews & Wilson 1997, 2000) properties of equal-mass neutron-star binaries were computed as a function of mass and EOS (Equation of State). From these studies it was deduced that compression, heating and collapse could occur at times from a few seconds to tens of seconds before binary merger. Our calculation of the rates of released binding energy and neutron star cooling suggests that interior temperatures as hot as 70 MeV are achieved. This leads to a high neutrino luminosity which peaks at $L_\nu \sim 10^{53}$ ergs sec $^{-1}$. This much neutrino luminosity would partially convert to an e^+e^- pair plasma above the stars as is also observed above the nascent neutron star in supernova simulations (Wilson & Mayle 1993).

We should point out, however, that many papers have been published claiming the compression is nonexistent. In Mathews et al. (1998) we presented a rebuttal to the critics. Subsequently, however, Flanagan (1999) pointed out a spurious term in our formula for the momentum constraint. We (Mathews & Wilson 2000) have corrected the momentum constraint equation and redone a sequence of calculations for a binary neutron star system with various angular momenta. A compression effect still exists which is able to release 10^{52} - 10^{53} ergs of gravitational binding energy. The compression does not occur for corotating stars with a polytropic equation of state. For irrotational binary stars our compression effect is consistent with the results of at least two other groups (Bonazzola et al. 1999a,b; Marronetti et al. 1999; Uryu & Eriguchi 1999) using different numerical methods to compute the relativistic hydrostatic equilibrium (Bonazzola et al. 1997). However, these calculations were done with a polytropic equation of state and found only very small compression; much less than 1%. For the polytropic equation of state Mathews & Wilson (2000) also found a compression less than 1%. In simulations with the realistic, somewhat soft, EOS described below we found clear evidence (Mathews & Wilson 2000) that significant compression, heating and collapse still occurs for sufficiently close orbits. The reason for this EOS dependence is straightforward. Table 1 shows the realistic EOS used in the present work and the (Mathews & Wilson 2000) studies. The key difference between the polytropic and realistic EOSs is that the adiabatic index Γ is not constant but decreases at low density for a realistic EOS. This causes the outer regions of the star to be more compact, and therefore, less affected by tidal stabilization than for polytropes. At the same time, the maximum central density tends to be larger for a neutron star of a fixed baryon mass. Therefore the relativistic effects are more dramatic when a realistic EOS is employed.

The hydrodynamic calculations that demonstrate compression have been made with the stars constrained to remain at zero temperature (i.e. efficient radiators). As the compression rate increases, however, it is expected that the rate of released binding energy will exceed the ability of

the star to radiate and internal heating will result. Large scale off-center vortices are observed to form (Mathews et al. 1998) within the stars with a characteristic circulation time scale of ~ 0.005 sec. The maximum velocities are nearly sonic. Among other things, this circulatory motion should help dissipate the compressional motion into thermal energy by shocks thereby heating the interior of the stars.

We have run several sets of calculations with realistic neutron-star equations of state. We first considered stars like our earlier bench mark cases (Mathews et al. 1998) with a baryon mass of $1.548 M_{\odot}$ corresponding to a typical (cf. Appendix A) gravitational mass of $M_G = 1.39 M_{\odot}$ and a central density of $\rho_c = 1.34 \times 10^{15}$ g cm $^{-3}$ in isolation. These stars are based upon the “realistic” EOS of table 1 for which the maximum critical mass is $M_c = 1.575 M_{\odot}$. As summarized in Appendix A, this maximum mass is typical of the somewhat soft EOS’s in which relativistic particles and/or condensates have been included. Parameters for this EOS were motivated by the necessity of such a soft EOS to obtain the correct neutrino signal in simulations of SN 1987A (Wilson & Mayle 1993). As noted in Table 5 of the Appendix this maximum mass is consistent with the measured masses of all binary pulsar systems for which the orbits have been well determined.

As noted above, the stars calculated using this realistic EOS show significant compression and released binding energy before inspiral but do not individually collapse. The released gravitational energy from this calculation is summarized in Table 2. Even without the collapse instability enough internal heating occurs to produce a significant gamma-ray burst.

We also found (Mathews & Wilson 2000) that the individual collapse of stars would occur if the stars are increased in mass from $M_G = 1.39$ to $1.44 M_{\odot}$ ($M_B = 1.61 M_{\odot}$) for this EOS. Collapse of this star system is observed to occur for very close separation ($d = 2.4R$) near (but before) the final stable orbit. Thus, collapse is a reasonable possibility for typical masses and a moderately soft EOS. For example, collapse would always occur prior to inspiral for stars in the typically observed mass range modeled with the EOS of Bethe & Brown (1995). For a critical mass of 1.54, even stars of initial mass of 1.35 collapse before reaching the innermost stable orbit.

Based upon the above results, we model the thermal energy deposition due to neutron star compression as follows: we expect that the fluid motion within the stars will quickly convert released gravitational binding energy into thermal energy in the interior of the stars. Thus, we estimate that the rate of thermal energy deposition is comparable to the rate of released binding energy due to compression. The amount of released binding energy scales with the orbital four velocity (Mathews & Wilson 1997, 2000). An estimate of the rate of increase of the orbital four velocity can be obtained (Mathews & Wilson 1997) from the gravitational radiation timescale. Then, from the relation between released binding energy and increasing four velocity (Mathews & Wilson 1997, 2000), the energy deposition rate into the stars can be deduced in approximate analytic form (Mathews & Wilson 1997). We write,

$$\dot{E}_{th} = \frac{(32/5)(Mf)^{5/3} f E_{th}^0}{[1 - (64/5)(Mf)^{5/3} ft]^{3/2}} , \quad (1)$$

where f is the orbital angular frequency and E_{th}^0 is the total thermal energy deposited into the stars. In the hydrodynamic pair plasma discussions below we consider a range of deposited thermal energy of $E_{th}^0 = 10^{51}, 10^{52}, 10^{53}$ ergs, consistent with the hydrodynamics simulations. We use the convention that $t < 0$ and $t = 0$ is the end of energy deposition when the neutron stars either have collapsed into two black holes or have reached the last stable orbit and collapsed to a single black hole. At the time that a typical neutron star binary system is near the last stable orbit, the orbital frequency is \sim a few $\times 10^3$ sec $^{-1}$. Hence, by Equation (1), the energy deposition rate would be

$$\dot{E}_{th} \approx 10^2 \times E_{th}^0 \text{ erg sec}^{-1} . \quad (2)$$

Thus, for $E_{th}^0 = 2 \times 10^{52}$ ergs, $\dot{E}_{th} \approx 2 \times 10^{54}$ ergs sec $^{-1}$.

The magnitude of the neutrino luminosity is very critical since the subsequent fireball is formed by neutrino-antineutrino annihilation. In order to model the thermal energy emitted by neutrinos before either stellar or orbital collapse we have constructed a computer model which treats the diffusion of energy in a static neutron star. This energy transport occurs by a combination of neutrino diffusion plus energy diffusion via a convective velocity-dependent diffusion coefficient. For the neutrino energy diffusion we write:

$$\frac{dE_\nu}{dt} = \vec{\nabla} \cdot D_\nu \vec{\nabla} E_\nu \quad (3)$$

where the coefficient for neutrino diffusion is just the form,

$$D_\nu^{rad} = \frac{c}{3\rho\kappa_\nu} + \frac{RV_c}{3} , \quad (4)$$

where a simple estimate for the neutrino opacity κ_ν is used, $\kappa_\nu \approx 9 \times 10^{43} T_{MeV}^2 \text{ cm}^2 \text{ g}^{-1}$ based upon the cross section for neutrino nuclear absorption and scattering. Characteristic convective velocities V_c were deduced from simulations using our three-dimensional binary neutron star code (Mathews & Wilson 2000). We calculated an angle averaged radial component of the fluid velocity in the frame of the star,

$$V_c = \frac{1}{4\pi} \int |V_r| d(\cos \theta) d\phi . \quad (5)$$

For our studies, these velocities were fit with an ansatz of the form

$$V_c \equiv \frac{32}{105} V_{c,ave} \frac{r}{R} \sqrt{1 - r/R} , \quad (6)$$

where r is the radial position inside a star of radius R and $V_{c,ave}$ is the volume averaged V_c . This gives a good fit to the numerical results and has the correct form in that the velocity goes to zero at the surface and also at $r = 0$.

Energy was deposited in accordance with equation 1 and the calculations terminated at time=0. In Figure 1 the fraction of energy released, the peak luminosity, and \bar{L} the average luminosity

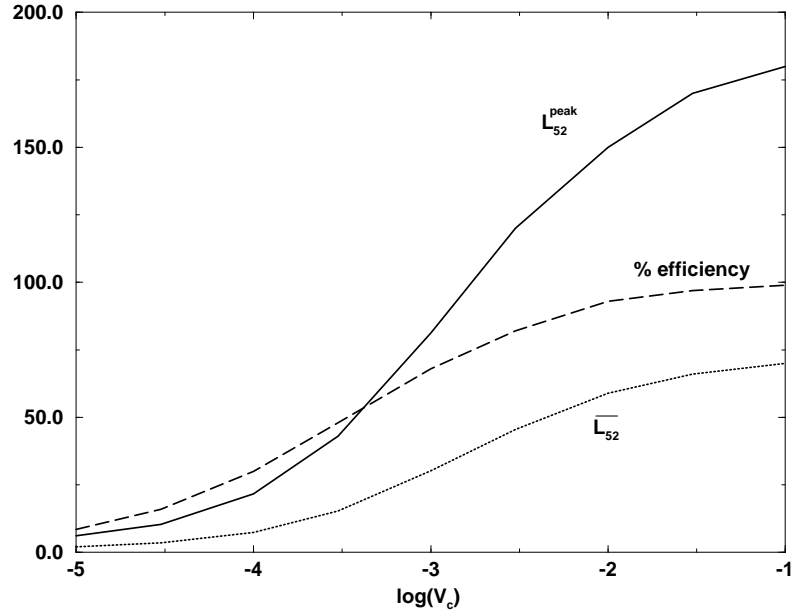


Fig. 1.— Luminosity from a compressed, heated neutron star as a function of average convective velocity within the star. Convection substantially improves the efficiency of transport of energy to the surface.

weighted by $L^{5/4}$ (see next section) are shown. The Energy input was 2×10^{52} ergs and the orbital frequency was 4000 rad sec $^{-1}$ (see Mathews & Wilson 2000). The average convective velocity was found to be $\approx 0.003 c$ by analyzing the hydrodynamical calculations Mathews & Wilson (2000) of neutron star binaries. From Figure 1 we see that a high emission efficiency and luminosity are obtained from this convective velocity. These produced lower thermal energies but about the same fraction of the energy emitted, $\approx 68\%$, but the \bar{L} is reduced. For $E_{th}^0 = 0.5$ (1.0) $\times 10^{52}$ ergs $\bar{L} = 0.75$ (1.5) $\times 10^{53}$ ergs sec $^{-1}$. From these calculations we estimate that the conversion of compressional energy to fireball energy is probably $\gtrsim 20\%$.

3. Neutrino Annihilation and Pair Creation

In the previous section we have outlined a mechanism by which neutrino luminosities of $\sim 10^{53}$ erg sec $^{-1}$ may arise from binary neutron stars approaching their final orbits. Here we argue that the efficiency for converting these neutrinos into pair plasma is probably quite high. Neutrinos emerging from the stars will deposit energy outside the stars predominantly by $\nu\bar{\nu}$ annihilation to form electron pairs. A secondary mechanism for energy deposition is the scattering of neutrinos from the e^+e^- pairs. Strong gravitational fields near the stars will bend the neutrino trajectories. This greatly enhances the annihilation and scattering rates (Salmonson & Wilson 1999). Figure 2

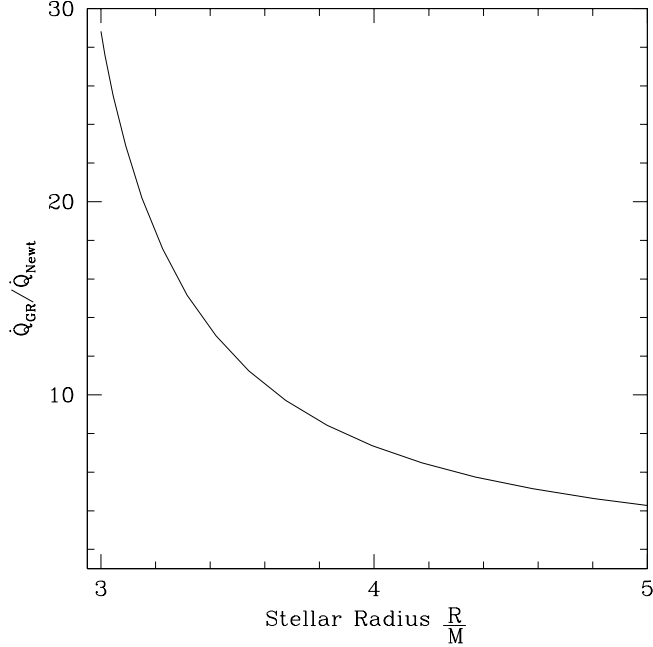


Fig. 2.— General relativistic neutrino heating augmentation $\mathcal{F} \equiv \dot{Q}_{GR}/\dot{Q}_{Newt}$ as a function of neutron star neutrinosphere radius down to $R = 3M$, where general relativistic energy deposition is \dot{Q}_{GR} , and Newtonian energy deposition is \dot{Q}_{Newt} .

taken from Salmonson & Wilson (1999) shows the relativistic enhancement factor, $\mathcal{F}(R/M)$, of the rate of annihilation by gravitational bending versus the radius to mass ratio (in units $G = c = 1$). For our employed neutron-star equations of state the radius to mass ratio is typically between $R/M \sim 3$ and 4 just before stellar collapse. Thus, the enhancement factor ranges from ~ 8 to 28. Defining the efficiency of energy deposition as the ratio of energy deposition to neutrino luminosity, then from Equation 24 of Salmonson & Wilson (1999) we obtain,

$$\frac{\dot{Q}}{L_\nu} \approx 0.03\mathcal{F}(R/M)L_{53}^{5/4} . \quad (7)$$

Thus, the efficiency of annihilation ranges from ≈ 0.1 to $0.84 \times L_{53}^{5/4}$. For the upper range of luminosity the efficiency is quite large.

To better analyze the annihilation process we have adapted the Mayle-Wilson (Wilson & Mayle 1993) supernova model to this problem. We emphasize that the Mayle-Wilson model is fully general relativistic. To investigate this problem, a hot neutron star of the appropriate R/M was constructed and the internal temperature adjusted to achieve the correct neutrino luminosities. The Courant condition requires that the time steps be quite small ($\sim 10^{-9}$ second), and zonal masses as low as $10^{-13}M_\odot$ are required just outside of the neutrinosphere. Hence, the calculations could only be evolved for a short time. The entropy per baryon s/k of the e^+e^- pair plasma is the critical

quantity for gamma-ray production. It can be written,

$$s/k = \frac{4m_b c^2 (ae^3)^{1/4}}{3k\rho} , \quad (8)$$

where ρ is the baryon density and e is the total energy density. The entropy per baryon was found to be in the range of $10^5 - 10^6$ for the high luminosities. For a luminosity of 10^{53} ergs sec $^{-1}$, an efficiency of energy transfer from the neutrinos to the e^+e^- pair plasma due to annihilation and electron scattering was found to be about 50 %. This efficiency of neutrino annihilation determines the total energy of the pair plasma and the entropy. This provides the initial conditions for the subsequent fireball expansion.

4. Pair Plasma Expansion

Having determined the initial conditions of the hot e^+e^- pair plasma near the surface of a neutron star, we wish to follow its evolution and characterize the observable gamma-ray emission. To study this we have developed a spherically symmetric, general relativistic hydrodynamic computer code to track the flow of baryons, e^+e^- pairs, and photons. For the present discussion we consider the plasma deposited at the surface of a $1.45M_\odot$ neutron star with a radius of 10 km.

The fluid is modeled by evolving the following spherically symmetric general relativistic hydrodynamic equations:

$$\frac{\partial D}{\partial t} = -\frac{\alpha}{r^2} \frac{\partial}{\partial r} \left(\frac{r^2}{\alpha} DV^r \right) + \dot{D}_{in} \quad (9)$$

$$\frac{\partial E}{\partial t} = -\frac{\alpha}{r^2} \frac{\partial}{\partial r} \left(\frac{r^2}{\alpha} EV^r \right) - P \left[\frac{\partial W}{\partial t} + \frac{\alpha}{r^2} \frac{\partial}{\partial r} \left(\frac{r^2}{\alpha} WV^r \right) \right] + \dot{E}_{in} \quad (10)$$

$$\frac{\partial S_r}{\partial t} = -\frac{\alpha}{r^2} \frac{\partial}{\partial r} \left(\frac{r^2}{\alpha} S_r V^r \right) - \alpha \frac{\partial P}{\partial r} - \alpha \frac{M}{r^2} \left(\frac{D + \Gamma E}{W} \right) \left[\left(\frac{W}{\alpha} \right)^2 + \frac{(U^r)^2}{\alpha^4} \right] \quad (11)$$

where $D = \rho W$ and $E = \epsilon \rho W$ are the Lorentz contracted coordinate densities of baryonic and thermal mass energy (e^+e^- and photons) respectively. The quantities \dot{D}_{in} and \dot{E}_{in} refer to the injected plasma from neutrino pair annihilation, and S_r is the radial coordinate momentum density. U^r is the radial component of the covariant 4-velocity. $W \equiv \alpha U^t$ is the generalized Lorentz factor, V^r is the radial coordinate three velocity, and Γ is an equation of state index. These quantities are

defined by

$$\begin{aligned} \alpha &\equiv \sqrt{1 - \frac{2M}{r}} \quad ; \quad U_r \equiv \frac{S_r}{D + \Gamma E} \quad ; \quad W \equiv \sqrt{1 + U^r U_r} \\ V^r &\equiv \frac{U^r}{W} \quad ; \quad \Gamma \equiv 1 + \frac{PW}{E} \end{aligned} \quad (12)$$

To evolve the e^+e^- pair plasma, we define a pair equation. The observed pair annihilation rate must be corrected for relativistic effects; specifically, time dilation slows the apparent pair annihilation process for a fast moving fluid with respect to an observer. Thus, we construct a continuity equation analogous to Equation (9) and add a term to account for annihilation and pair-production reactions:

$$\frac{\partial N_{pairs}}{\partial t} = -\frac{\alpha}{r^2} \frac{\partial}{\partial r} \left(\frac{r^2}{\alpha} N_{pairs} V^r \right) + \bar{\sigma} \bar{v} ((N_{pairs}^0(T))^2 - N_{pairs}^2) / W^2 . \quad (13)$$

Here, N_{pairs} is the coordinate pair number density, and $\bar{\sigma} \bar{v}$ is the Maxwellian averaged mean pair annihilation rate per particle. Although $\bar{\sigma} \bar{v}$ depends on T , it varies little in the temperature range of interest, and thus, can be taken as constant: $\bar{\sigma} \bar{v} = 2.5 \times 10^{-25} \text{ cm}^3 \text{ sec}^{-1}$. $N_{pairs}^0(T) = n_{pairs}^0(T)W$, where $n_{pairs}^0(T)$ is the local proper equilibrium e^+e^- pair density at temperature T given by the appropriate Fermi integral with a chemical potential of zero. Zero chemical potential is a good approximation when $N_{pairs}^0(T)$ of Equation (13) is important.

The total proper energy equation, including photons and e^+e^- pairs (baryon thermal energy is negligible), is

$$e_{tot} = aT^4 + e_{pairs} \quad (14)$$

where coordinate energy in Equation (10) is related to proper energy by $E = e_{tot}W$ and e_{pairs} is the appropriate zero chemical potential Fermi integral normalized to give the proper e^+e^- pair density $n_{pair} = N_{pairs}/W$ as determined by Equation (13).

The entropy per baryon (Equation 8) of the wind is crucial to the behavior of the burst. An entropy that is too high will create a burst which is much hotter than those observed, while an entropy that is too low will extinguish the burst with baryons. We find that entropies of the order 10^7 to 10^8 are ideal for producing an isotropic burst directly from the expanding pair-photon plasma. In the calculations shown below (Sections 5 & 6) we cover a range of possible entropies per baryon from 10^6 to 10^8 . Other possible sources of high entropy-per-baryon plasmas include the formation of magnetized black holes (Ruffini et al. 1998, 1999) and the high-energy collisions ($\gamma \approx 2$) of stars in collapsing globular clusters, which we are studying in a separate work.

We will deal with two paradigms for γ -ray production. First, we treat the high entropy case ($s/k > 10^7$) where the emission is from the fireball. Secondly, we present a low entropy case in which gamma emission arises from the collision of the fireball with the local interstellar medium.

In the first case, the hydrodynamic equations are evolved as the plasma expands. Once the system becomes transparent to Thomson scattering, ($\int N_{pair}(r) \sigma_T dr \lesssim 1$ where σ_T is the Thomson

cross-section) we assume the photons are free-streaming, the calculation is stopped and the photon gas is analyzed to determine the photon signal.

5. Analysis of the Spectrum and Light curve

We find that the photons and e^+e^- pairs appear to decouple at virtually the same time throughout the entire photon- e^+e^- pair plasma (when the cloud has reached a radius $\sim 10^{12} - 10^{13}$ cm and the temperature is typically a few 10's of eV). As such, the photons will be well approximated as thermal and so we neglect any radiation transport effects. Thus, we take decoupling to be instantaneous and to occur when the plasma becomes optically thin to Thomson scattering. Furthermore, we find that virtually none of the energy deposited in the e^+e^- pair plasma remains in the pairs ($\sim .001\%$). Thus, the conversion of e^+e^- pair energy to photons and baryons is very efficient. From this simulation we derive two observables, the time integrated energy spectrum $N(\epsilon)$ and the total energy received as a function of observer time $\varepsilon(t)$.

5.1. The Spectrum

As mentioned above, we assume that the e^+e^- pairs and photons are equilibrated to the same T when they decouple. Thus, the photons in the fluid frame (denoted with a prime: $'$) make up a Planck distribution of the form

$$u'_{\epsilon'}(T') \approx \frac{\epsilon'^3}{\exp(\epsilon'/T') - 1} , \quad (15)$$

but u_{ϵ}/ϵ^3 is a relativistic invariant (Rybicki & Lightman 1975). This implies ϵ/T is also a relativistic invariant. So a Planck distribution in an emitter's rest-frame with temperature T' will appear Planckian to a moving observer, but with boosted temperature $T = T' / (\gamma(1 - v \cos \theta))$ where $v \cos \theta$ is the component of fluid velocity ($c=1$) directed toward the observer. Thus,

$$u_{\epsilon}(\theta, v, T') \approx \frac{\epsilon^3}{\exp(\gamma(1 - v \cos \theta) \frac{\epsilon}{T'}) - 1} \quad (16)$$

gives the observed spectrum of a blackbody with rest-frame temperature T' moving at velocity v and angle θ with respect to the observer.

In the present case we wish to calculate the spectrum from a spherical, relativistically expanding shell as seen by a distant observer. Since we know v , T' and the radius R of the shell, we integrate over volume (i.e., shell, angle) with respect to the observer. We thus obtain the observed photon energy spectrum $N_{\epsilon} = \int (u_{\epsilon}/\epsilon) d^3x$, from a relativistically expanding spherical shell with radius R , thickness dR , velocity v , Lorentz factor γ and fluid-frame temperature T' , to be (in

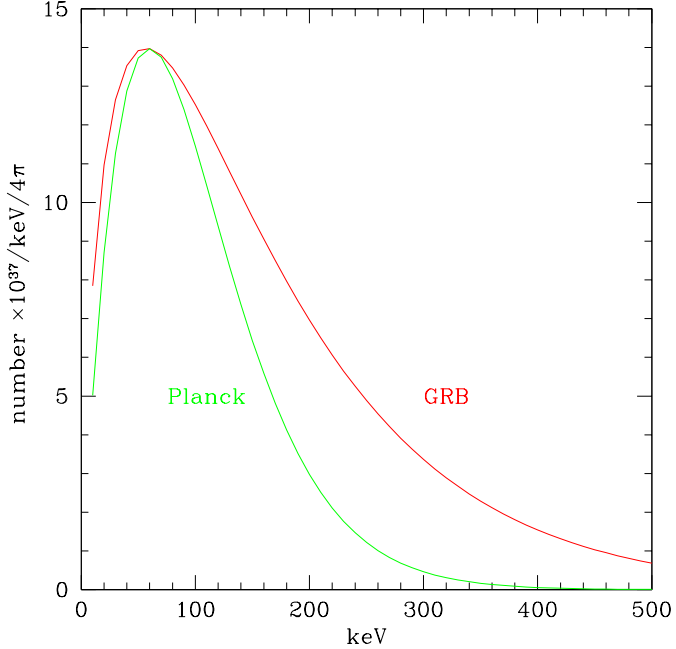


Fig. 3.— A spectrum of a relativistically expanding spherical fireball. A Planck spectrum is shown for reference to show that the gamma-ray burst spectrum is not a black-body out to several 100 keV.

photons/eV/steradian)

$$N_\epsilon(v, T', R) = (5.23 \times 10^{11}) 4\pi R^2 dR \frac{\epsilon T'}{v\gamma} \log \left[\frac{1 - \exp[-\gamma\epsilon(1+v)/T']}{1 - \exp[-\gamma\epsilon(1-v)/T']} \right] \text{ (eV}^{-1}\text{sr}^{-1}), \quad (17)$$

where R is in cm. Note, that this spectrum has a maximum at $\epsilon_{max} \cong 1.39\gamma T' \text{ eV}$ for $\gamma \gg 1$. We may then sum this spectrum over all shells (the zones in our computer code) of the fireball to get the total spectrum. Figure 3 shows an example of such a spectrum up to 500 keV. Since we assume *a priori* that the photons are thermal, our spectrum has a high frequency exponential tail, but the resultant total spectrum is clearly not thermal in the high energies.

5.2. The Light Curve

To construct the observed light curve $\varepsilon(t)$ we again decompose the spherical plasma into concentric shells and consider two effects: First, is the relative arrival time of the first light from each shell: light from outer shells will be observed before light from inner shells; Second, is the shape of the light curve from a single shell.

Emission from moving pair plasma is beamed along the direction of travel within an angle

$\theta \sim 1/\gamma$. The surface of simultaneity of a relativistically expanding spherical shell, as seen by an observer, is an ellipsoid (Fenimore et al. 1996). The observer time of intersection of an expanding ellipse with a fixed shell of radius R as a function of θ (i.e. the time at which emission from this intersection circle is received) is:

$$t = \frac{R}{v}(1 - v \cos \theta) \cong \frac{R}{2\gamma^2 c} , \quad (18)$$

for $\theta \ll 1, \gamma \gg 1$. Integrating our boosted Planck distribution of photons (Equation 16) over frequency, we find that a relativistically expanding shell of radius R will have a time profile (energy/time/steradian)

$$\varepsilon(\tau, v, T', R) = \frac{a}{2} \left(\frac{T'}{\gamma \tau} \right)^4 c R dR \sim 1/\tau^4 , \quad (19)$$

for $\tau > 1$ and where $\tau \equiv \frac{vt}{R}$. Emission starts at $\tau_i = (1 - v/c)$ and ends at $\tau_f = (1 + v/c)$. The final light curve is constructed by summing the signal from all shells. The total thickness of the expanding plasma is $\sim cJ/\dot{J}$ because it expands at near the speed of light and J/\dot{J} is the timescale of compression and coalescence which sets the emission timescale. Typically $R \sim 10^{12}$ cm and $J/\dot{J} \sim$ a few seconds, so $cJ/\dot{J} \ll R$ and the emitting plasma is a thin shell. The duration of the burst is determined by the duration of emission because the observed timescale of emission from the plasma shell is very short, $R/2\gamma^2 c \sim 0.01$ seconds (Equation 18) for $\gamma \sim 100$, compared to J/\dot{J} .

6. Results of Pair Plasma Emission

We have run a variety of models over a range of entropies per baryon and total energies. The results are summarized in Figures 4, 5 & 6. We see that more powerful bursts are derived from higher entropies per baryon and higher total energies. In particular, entropies per baryon of a few $\times 10^7$ allow a burst with a spectral peak ~ 100 keV and efficiencies $E_\gamma/E_{tot} \sim 10\%$. This is consistent with, although at the upper end of the range of, the entropies calculated for the e^+e^- plasma deposited above the neutron stars. Much further work needs to be done to better characterize the nature of the stellar compression and energy transport within the stars. Also, more elaborate simulations must be done to resolve the plasma flow in three dimensions and to consider the effects of magnetic fields. In Table 3 we see the final Lorentz factor for a range of expanding fireballs. This data will be used when we look at the collision of the fireball into an external medium.

7. External Shock Emission

In previous sections the emission from an expanding fireball was studied. We found that the resulting emission spectrum and total energy strongly depends upon the energy of the plasma

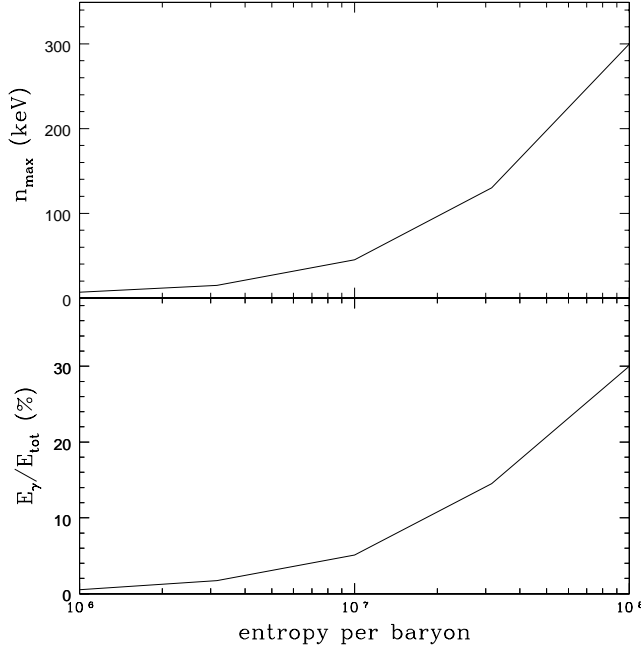


Fig. 4.— The photon energy at the spectrum peak, and gamma-ray efficiency are plotted for a total energy $E_{tot} = 10^{52}$ ergs over a range of entropies 10^6 to 10^8 .

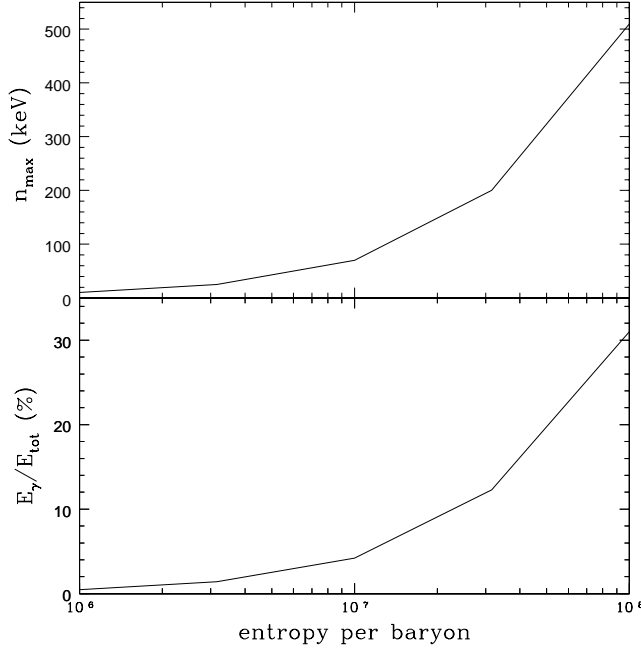


Fig. 5.— The photon energy at the spectrum peak, and gamma-ray efficiency are plotted for a total energy $E_{tot} = 10^{53}$ ergs over a range of entropies 10^6 to 10^8 .

deposited near the surface of the neutron stars; entropies of $\lesssim 10^6$ resulted in weak emission with most of the original energy manifesting itself as kinetic energy of the baryons. Thus, for the low entropy per baryon fireballs ($s \sim 10^5 - 10^6$) produced by NSBs it is necessary to examine the emission due to the interaction of the relativistically expanding baryon wind with the interstellar medium (ISM).

After becoming optically thin and decoupling with the photons, the matter component of the fireball continues to expand and interact with the ISM via collisionless shocks. As the ISM is swept up, the matter decelerates. We model this process as an inelastic collision between the expanding fireball and the ISM as in, for example, Piran (1999). We assume that the absorbed internal energy is immediately radiated away. From this we construct a simple picture of the emission due to the matter component of the fireball “snowplowing” into the ISM of baryon number density n .

For a shell of a given rest mass M expanding at Lorentz factor γ , the conservation of momentum leads to the following constraint equation:

$$\frac{d\gamma}{\gamma^2 - 1} = -\frac{dM}{M}, \quad (20)$$

which has the solution

$$\frac{M}{M_0} = \sqrt{\frac{(\gamma_0 - 1)(\gamma + 1)}{(\gamma_0 + 1)(\gamma - 1)}}. \quad (21)$$

Now we can put this in terms of radius by noting

$$M = M_0 + \frac{4\pi}{3} n m_p c^2 R^3. \quad (22)$$

Thus,

$$R(\gamma) = R_0 \left(\frac{M}{M_0} - 1 \right)^{1/3} \cong R_0 \left(\frac{1}{\gamma} - \frac{1}{\gamma_0} \right)^{1/3} \quad \text{for } \gamma, \gamma_0 \gg 1, \quad (23)$$

where

$$R_0 \equiv \sqrt[3]{\frac{3M_0}{4\pi n m_p c^2}}, \quad (24)$$

is the radius at which $M = 2M_0$. This is the characteristic radius at which the shock decelerates.

We assume that the local thermal energy radiated away after a thin shell of ISM mass dM is swept up by the shock is

$$dE' = (\gamma - 1)dM. \quad (25)$$

The observer time elapsed for the mass to expand a distance dR is

$$dt_{obs} = \frac{dR}{2\gamma^2 c}. \quad (26)$$

Equations (23,26) can be solved in the relativistic limit to give

$$t(\gamma, \gamma_0) \cong \frac{R_0}{28c} \left(\frac{9}{\gamma_0^2} + \frac{3}{\gamma\gamma_0} + \frac{2}{\gamma^2} \right) \left(\frac{1}{\gamma} - \frac{1}{\gamma_0} \right)^{1/3} \quad \text{for } \gamma, \gamma_0 \gg 1 . \quad (27)$$

The implied observer luminosity, from Equations (26, 25), is

$$L = \frac{dE}{dt_{obs}} = \frac{\gamma dE'}{dt_{obs}} \approx 8\pi R^2 \gamma^4 n m_p c^3 \quad (28)$$

for $\gamma \gg 1$. Using Equation (27), a relativistic ($\gamma \gg 1$) solution for observed luminosity, in ergs sec $^{-1}$, over several epochs is

$$L(t) \cong \begin{cases} 2.68 \times 10^{50} n \gamma_{300}^8 t^2 (1 - 6.27 \times 10^{-3} \gamma_{300}^8 n E_{52}^{-1} t^3)^{10/3} & t < t_1 \\ 7.88 \times 10^{51} n^{1/3} E_{52}^{2/3} \gamma_{300}^{8/3} (0.32 \frac{t}{t_{max}} - 0.15)^{2/3} (1.15 - 0.32 \frac{t}{t_{max}})^{10/3} & t_1 < t < t_2 \\ 5.3 \times 10^{51} n \gamma_{300}^4 \left[\frac{E_{52}}{n \gamma_{300}} \right]^{4/7} t^{2/7} (1 - \sqrt{f(t)})^4 (f(t) + \sqrt{f(t)})^{2/3} & t > t_2 \end{cases} \quad (29)$$

where constant parameters are, $E_{52} \equiv E/10^{52}$ ergs, $\gamma_{300} \equiv \gamma_0/300$ and n is in baryons cm $^{-3}$. For $t > t_2$:

$$f(t) \equiv 1 - 1.05 \left(\frac{t_{max}}{t} \right)^{3/7} \quad (30)$$

and

$$t_{max} \equiv 3.5 \sqrt[3]{\frac{E_{52}}{n \gamma_{300}^8}} \quad \text{seconds} \quad (31)$$

is the observer time at maximum luminosity L_{max} :

$$L(t_{max}) = L_{max} = 1.3 \times 10^{51} n^{1/3} \gamma_{300}^{8/3} E_{52}^{2/3} \quad \text{ergs/sec} . \quad (32)$$

The times at which the solutions for each epoch are spliced together are roughly

$$t_1 \sim 0.6 t_{max} \quad (33)$$

$$t_2 \sim 1.5 t_{max} . \quad (34)$$

Figure 7 shows the light curve for a 10^{52} erg fireball expanding at $\gamma = 300$ for a range of ISM densities. This corresponds to an initial energy deposition above the neutron stars with an entropy per baryon of $s = 10^5$ as seen in Table 3. The expansion can be divided into a free-expansion phase and a deceleration phase:

$$L(t) \propto \begin{cases} t^2 & \text{free expansion phase } (t < t_{max}) \\ t^{-10/7} & \text{deceleration phase } (t > t_{max}) \end{cases} \quad (35)$$

Figure 8 shows a linear plot of the light curve for ISM density $n = 1.0$ baryons cm $^{-3}$. The “fast-rise, exponential-decay” or “FRED”-like shape is evident and is in good qualitative agreement with “smooth” GRBs.

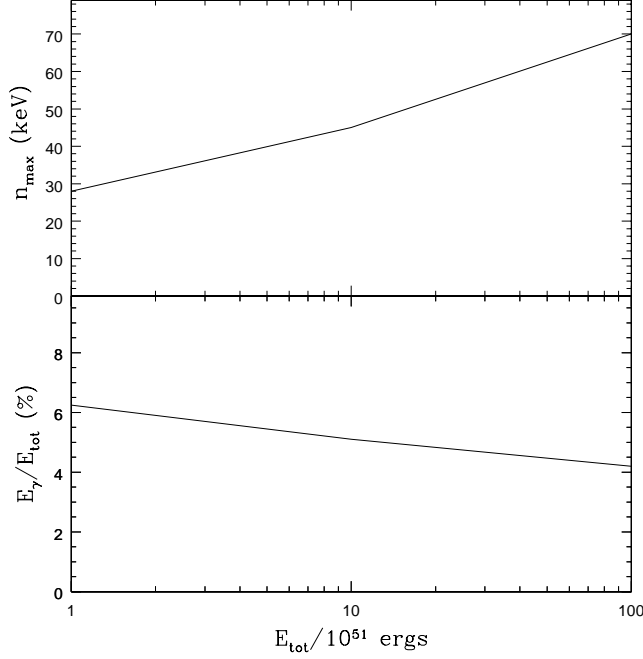


Fig. 6.— The photon energy at the spectrum peak, and gamma-ray efficiency are plotted for an entropy per baryon $s = 10^7$ over a range of energies 10^{51} to 10^{53} ergs.

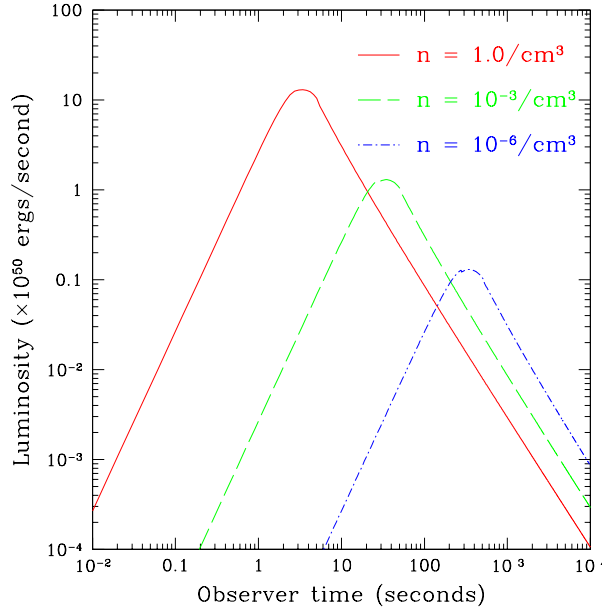


Fig. 7.— The light curve for a 10^{52} erg fireball expanding at $\gamma = 300$ into interstellar media with three different baryon number densities n .

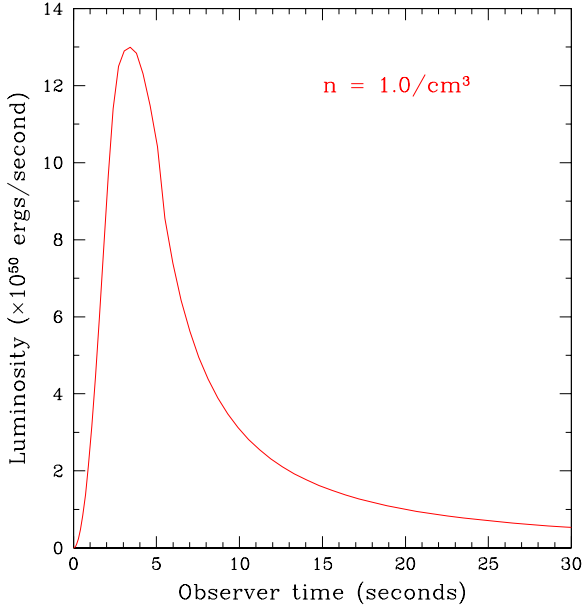


Fig. 8.— The light curve for a 10^{52} erg fireball expanding at $\gamma = 300$ into interstellar media with baryon density $n = 1.0 \text{ cm}^{-3}$. This curve is similar in its “fast-rise, exponential decay” shape and ~ 10 second duration to the light curves of many of the smooth-type GRBs.

7.1. Synchrotron Shock Spectrum

Now we wish to model the spectrum of light emitted as the fireball expands into the ISM. To do this we assume an external synchrotron shock model (Shemi & Piran 1990; Rees & Mészáros 1992; Mészáros & Rees 1993; Rees & Mészáros 1994). This analysis is analogous to afterglow models in the radiative limit. Thus, the spectrum will have the form (Sari et al. 1998)

$$L_\nu = \begin{cases} (\nu/\nu_c)^{1/3} L_{\nu,\max} & \nu < \nu_c \\ (\nu/\nu_c)^{-1/2} L_{\nu,\max} & \nu_m > \nu > \nu_c \\ (\nu_m/\nu_c)^{-1/2} (\nu/\nu_m)^{-p/2} L_{\nu,\max} & \nu > \nu_m \end{cases} \quad (36)$$

Photon frequency ν_m is the frequency corresponding to the minimum energy of the electron distribution above which the electrons are assumed to have a power law functional form $n(\gamma) \sim \gamma^{-p}$. In the numerical examples that follow, we take the spectral index to be $p = 2.5$. This is consistent with that calculated for ultrarelativistic shocks (Bednarz & Ostrowski 1998). The “cooling frequency” ν_c corresponds to the energy below which the electrons cannot cool on a hydrodynamic timescale. The peak of the luminosity spectrum is

$$L_{\nu,\max} \cong \left(\frac{p-2}{2p-2} \right) \frac{L}{\sqrt{\nu_m \nu_c}} , \quad (37)$$

assuming $\nu_m \gg \nu_c$, which is valid throughout the burst duration.

There are two free parameters in this model. ϵ_e is the fraction of the kinetic energy of the baryons that is deposited into the electrons by the shock. ϵ_B is the ratio of the magnetic field energy density to the kinetic energy density of the baryons. In these simulations we take each of these values to be 1/4.

The evolution of the characteristic frequency ν_m is described by

$$\nu_m \cong 1.4 \times 10^4 \epsilon_e^2 \epsilon_B^{1/2} \sqrt{n} \gamma_{300}^4 \text{ keV} \begin{cases} (1 - (\frac{2ct}{R_0})^3 \gamma_0^7)^4 & t < t_1 \\ (1.15 - 0.32t/t_{max})^4 & t_1 < t < t_2 \\ \left(1 - \sqrt{1 - \frac{2}{\gamma_0} (\frac{14ct}{R_0})^{-3/7}}\right)^4 & t > t_2 . \end{cases} \quad (38)$$

The behavior of the cooling frequency ν_c is more difficult to characterize since it depends on the hydrodynamical timescale of the fluid. Fortunately, however, ν_c is much smaller than ν_m . Therefore, its exact behavior is not important for this analysis. Thus, we assume ν_c to be constant at early times and follow its asymptotic power-law at later times:

$$\nu_c \cong 2.7 \times 10^{-3} \epsilon_B^{-3/2} E_{52}^{-4/7} \gamma_{300}^{4/7} n^{-13/14} \text{ keV} \begin{cases} t_{max}^{-2/7} & t \leq t_{max} \\ t^{-2/7} & t > t_{max} . \end{cases} \quad (39)$$

The spectrum of the burst at peak luminosity L_{max} is shown in Figure 9. For $n = 1.0$ baryons cm^{-3} , most of the energy is emitted at photon energies ~ 100 keV. Using Equations (29,38,39) for L , ν_m and ν_c respectively, we can determine the spectrum (Equation 36). The fluence spectrum of the burst is obtained by integrating the evolving luminosity spectrum (Equation 36) in time. This is shown in Figure 10. This figure again shows that most of the burst energy is in photons of several hundred keV energy.

Now we can ask what the efficiency is of gamma-ray production by the shock compared to other wavelengths. At any time, the fraction of luminosity above a given minimum frequency ν_{min} is

$$\varepsilon_{ff} = \begin{cases} \frac{\left[\left(\frac{2p-2}{p-2}\right)\nu_m^{-1/2} - 2\nu_{min}^{1/2}\right]}{\left[\left(\frac{2p-2}{p-2}\right)\nu_m^{-1/2} - \frac{5}{4}\nu_c^{1/2}\right]} & \nu_c < \nu_{min} < \nu_m \\ \frac{\left(\frac{2}{p-2}\right)\left(\frac{\nu_m^{p-1}}{\nu_{min}^{p-2}}\right)^{1/2}}{\left[\left(\frac{2p-2}{p-2}\right)\nu_m^{-1/2} - \frac{5}{4}\nu_c^{1/2}\right]} & \nu_{min} > \nu_c . \end{cases} \quad (40)$$

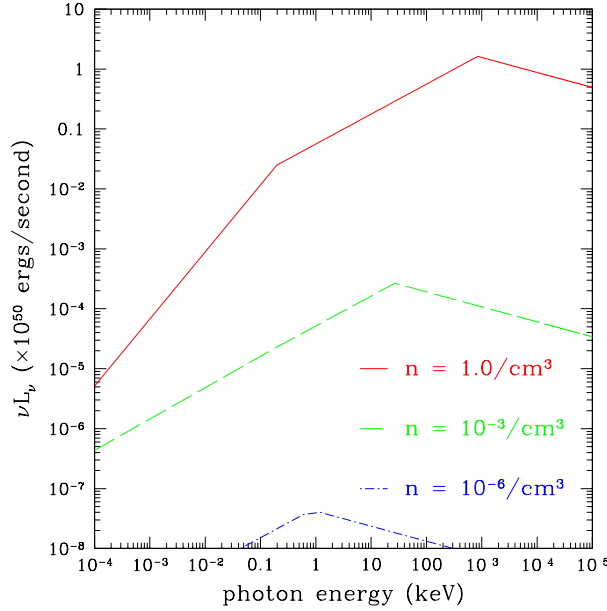


Fig. 9.— The synchrotron spectrum for a 10^{52} erg fireball expanding at $\gamma = 300$ into interstellar media with three different baryon number densities n .

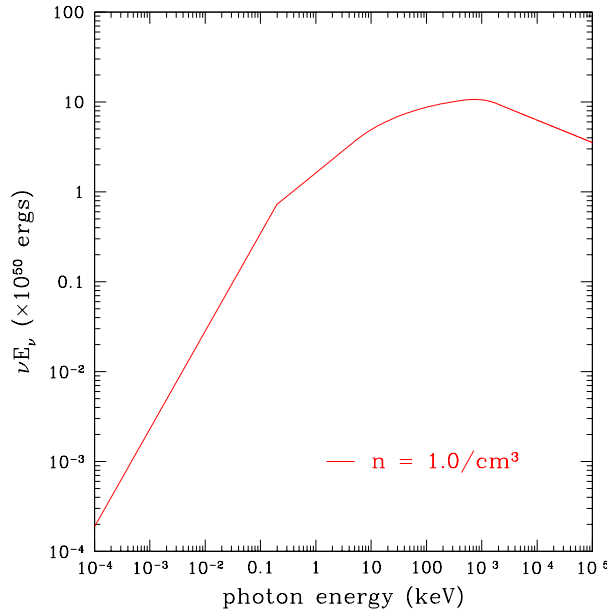


Fig. 10.— The total energy spectrum of a 10^{52} erg fireball expanding at $\gamma = 300$ into an interstellar medium with baryon number density $n = 1.0 \text{ cm}^{-3}$.

Thus, we can calculate the duration, t_{90} , of the luminosity at energies above this minimum energy. This is done in Table 4 for the various fireballs shown in Table 3. There is a competition between factors limiting the duration; lower energy fireballs simply have fewer high energy photons, and thus, shorter duration; while higher energy fireballs expand and evolve faster and thus have shorter duration. Fireballs with energy of order 10^{52} ergs and entropies per baryon of order 10^5 yield a value for t_{90} which is consistent with observation.

The overall efficiency of the production of photons above a frequency ν_{min} is

$$\begin{aligned} \varepsilon_{fftot} &\equiv \frac{\int_0^\infty \int_{\nu_{min}}^\infty L_\nu d\nu dt}{\int_0^\infty \int_0^\infty L_\nu d\nu dt} \\ &\approx 1 - \left(\frac{\nu_{min}}{\nu_{max}} \right)^{1/6} \quad \text{for } \nu_{min} \ll \nu_{max} , \end{aligned} \quad (41)$$

where ν_{max} is the value of ν_m (Equation 38) at $t = t_{max}$. For $\nu_{min} = 10$ keV we have an overall efficiency of about $\varepsilon_{fftot} \approx 75\%$. Thus, the radiative external shock GRB is quite efficient at producing gamma-rays if our assumptions are reasonable.

8. Conclusions

In this paper we have argued that heated neutron stars (perhaps by compression of close neutron-star binaries) are viable candidates for the production of large, high entropy per baryon, e^+e^- pair plasma fireballs, and thus, for the creation of gamma-ray bursts. We find that fireballs of total energy $E \sim 10^{51}$ to 3×10^{52} ergs and an entropy per baryon of $s/k \sim 10^5 - 10^6$ are possible. Values for the entropy as high as 10^7 may be realized during the peak $\nu\bar{\nu}$ luminosity (of $\approx 10^{53}$ ergs sec $^{-1}$). Emergent gamma-rays yield a quasi-thermal spectrum peaked at ~ 100 keV with an efficiency of conversion from pair plasma to photons of $\sim 30\%$. The lower entropy component of the fireball will initiate a shock which propagates into the ISM, generating an external shock GRB.

The calculation utilizing the supernova computer program (Section 3) to describe the neutrino and matter transport, produces a baryonic wind that contains $\sim 90\%$ neutrons. The decay of the neutrons to protons occurs on the same time scale as that for which the protons are decelerated by the intersteller medium. This delayed conversion of neutrons to protons will broaden the gamma-ray signal by a factor of a few. In addition, the decay electrons will strongly increase the entropy of the expanding plasma at the late times. In future work we will quantify the role of neutrons and explore the possibility of fireball photons inverse-Compton up-scattering off of the accelerated electron distribution of the external shock. This corresponds to the emission scenario put forward by Liang et al. (1997).

As of yet this model is spherically symmetric. Thus, it can only generate bursts with a smooth light-curve structure. However, we expect a large variety of GRB morphologies with varied time structure due to: 1) three dimensional resolution of the plasma flow; 2) plasma instabilities due to

increased heating of the deposited plasma with time; and 3) variation in the ratio of star mass in the NSB, effecting the relative compression and heating rate of each star.

In future work we will numerically model, in three dimensions, the flow of the e^+e^- pair plasma in the midst of the orbiting neutron stars. We have written a three-dimensional general relativistic hydrodynamic code to study this three-dimensional behavior. In particular, we wish to study the possible formation of jets along the orbital axis due to the collision of plasma blowing away from each star. Also, we have done simulations which suggest that the internal magnetic field of the neutron stars may be high. Thus, the inclusion of magnetohydrodynamic plasma effects including Alfvén instabilities and reconnections may ultimately be necessary.

The authors wish to thank the late Jean-Alain Marck for his inciteful and encouraging remarks on an earlier version of this manuscript. This work was performed under the auspices of the U.S. Department of Energy by University of California Lawrence Livermore National Laboratory under contract W-7405-ENG-48. J.R.W. was partly supported by NSF grant PHY-9401636. Work at University of Notre Dame supported in part by DOE grant DE-FG02-95ER40934, NSF grant PHY-97-22086, and by NASA CGRO grant NAG5-3818.

REFERENCES

- Akmal A., Pandharipande V. R., Ravenhall D. G. 1999, Phys. Rev. C, 58, 1804
An P., Lattimer J., Prakash M. 1998, BAAS, 192, 8207
Arnett W. D., Bowers R. L. 1977, Astrophys. J. Suppl. Ser., 33, 415
Bednarz J., Ostrowski M. 1998, Phys. Rev. Lett., 80(18)
Bethe H. A., Brown G. E. 1995, ApJ, 445, L29
Blaizot J. P. 1980, Phys. Rep., 64, 171
Bonazzola S., Gourgoulhon E., Marck J.-A. 1997, Phys. Rev. D, 56, 7740
Bonazzola S., Gourgoulhon E., Marck J.-A. 1999a, in Proceedings of the 19th Texas Symposium on Relativistic Astrophysics and Cosmology, held in Paris, France, Dec. 14-18, 1998. Eds.: J. Paul, T. Montmerle, and E. Aubourg (CEA Saclay).
Bonazzola S., Gourgoulhon E., Marck J.-A. 1999b, Phys. Rev. Lett., 82, 892
Brown G. E., Bethe H. A. 1994, ApJ, 423, 659
Collins T. J. B., Helfer H. L., Van Horn H. M. 1998, ApJ, 508, L159
Dermer C. D., Mitman K. E. 1999, ApJ, 513, L5

- Fenimore E. E., Madras C. D., Nayakshin S. 1996, *ApJ*, 473, 998
- Flanagan E. E. 1999, *Phys. Rev. Lett.*, 82(7), 1354
- Friedman J. L., Isper J. R., Parger L. 1986, *ApJ*, 304, 115
- Galama T. J., Groot P. J., Van Paradijs J., Kouveliotou C., Centurion M., Telting J. H. et al. 1997, *IAU Circ.*, 6655, 1
- Gotthelf E. V., Vasisht G., Dotani T. 1999, *ApJ*, 522, 115
- Groot P. J., Galama T. J., Van Paradijs J., Strom R., Telting J., Rutten R. G. M. et al. 1997, *IAU Circ.*, 6584, 1
- Haberl F. et al. 1997, *A&A*, 326, 662
- Janka H. T., Ruffert M. 1996, *A&A*, 307, L33
- Klebesadel R. W., Strong I. B., Olson R. A. 1973, *Astrophys. J. Lett.*, 182, L85
- Kobayashi S., Piran T., Sari R. 1998, in Huntsville Gamma-Ray Burst Symposium, p. 672
- Kouveliotou C. et al. 1998, *Nature*, 391, 235
- Kulkarni S. R., Frail D. A., Wieringa M. H., Ekers R. D., Sadler E. M., Wark R. M., Higdon J. L., Phinney E. S., Bloom J. S. 1998, *Nature*, 395, 663
- Lattimer J. M. 1998, in N. Shibasaki et al. (eds.), *Neutron Stars and Pulsars Thirty Years after the Discovery*, Universal Acadamy Press, Tokyo, Japan, p. 103
- Liang E., Kusunose M., Smith I. A., Crider A. 1997, *ApJ*, 479, L35
- Link B., Epstein R. L., Lattimer J. M. 1999, *Phys. Rev. Lett.*, 83, 3362
- Marronetti P., Mathews G. J., Wilson J. R. 1999, *Phys. Rev. D*, 60, 087301
- Mathews G. J., Marronetti P., Wilson J. R. 1998, *Phys. Rev. D*, 58, 043003
- Mathews G. J., Wilson J. R. 1997, *ApJ*, 482, 929
- Mathews G. J., Wilson J. R. 2000, *Phys. Rev. D*, 61, 127304
- McAbee T. L., Wilson J. R. 1994, *Nuclear Physics A*, 576, 626
- Meegan C. A., Fishman G. J., Wilson R. B., Horack J. M., Brock M. N., Paciesas W. S., Pendleton G. N., Kouveliotou C. 1992, *Nature*, 355, 143
- Merloni A., Vietri M., Stella L., Bini D. 1999, *MNRAS*, 304, 155
- Mészáros P., Rees M. J. 1993, *ApJ*, 405, 278

- Miller M. C., Lamb F. K., Psaltis D. 1998, *ApJ*, 508, 791
- Morsink S. M., Stella L. 1999, *ApJ*, 513, 827
- Page D. 1998, in N. Shibasaki et al. (eds.), *Neutron Stars and Pulsars Thirty Years after the Discovery*, Universal Acadamy Press, Tokyo, Japan, p. 183
- Piran T. 1999, *astro-ph/9907392*
- Rees M. J., Mészáros P. 1992, *MNRAS*, 258, 41P
- Rees M. J., Mészáros P. 1994, *ApJ*, 430, L93
- Ruffert M., Janka H.-T. 1998, *A&A*, 338, 535
- Ruffert M., Janka H.-T. 1999, *A&A*, 344, 573
- Ruffini R., Salmonson J. D., Wilson J. R., Xue S. S. 1998, in *Abstracts of the 19th Texas Symposium on Relativistic Astrophysics and Cosmology*, held in Paris, France, Dec. 14-18, 1998. Eds.: J. Paul, T. Montmerle, and E. Aubourg (CEA Saclay), p. E39
- Ruffini R., Salmonson J. D., Wilson J. R., Xue S. S. 1999, *A&A*, 350, 334
- Rybicki J. B., Lightman A. P. 1975, *Radiative Processes in Astrophysics*, USA: John Wiley & Sons, Inc.
- Salmonson J. D., Wilson J. R. 1999, *ApJ*, 517, 859
- Sari R., Piran T., Narayan R. 1998, *ApJ*, 497, L17
- Schaab C., Weigel M. K. 1999, *MNRAS*, 308, 718
- Shemi A., Piran T. 1990, *ApJ*, 365, L55
- Strohmayer T. E., Zhang W., Swank J. H., Smale A., Titarchuk L., Day C., Lee U. 1996, *ApJ*, 469, L9
- Thorsett S. E., Chakrabarty D. 1999, *ApJ*, 512, 288
- Titarchuk L., Osherovich V. 1999, *ApJ*, 518, L95
- Uryu K., Eriguchi Y. 1999, *Phys. Rev. D*, 61, 024039
- Van Der Klis M., Swank J. H., Zhang W., Jahoda K., Morgan E. H., Lewin W. H. G., Vaughan B., Van Paradijs J. 1996, *ApJ*, 469, L1
- Van Der Klis M., Wijnands R. A. D., Horne K., Chen W. 1997, *ApJ*, 481, L97
- Vietri M., Stella L. 1998, *ApJ*, 503, 350

- Walter F. M., Wolk S. J., Neuhauser R. 1996, *Nature*, 379, 233
- Wang J. C. L., Link B., Van Riper K., Arnaud K. A., Miralles J. A. 1999, *å*, 345, 869
- Wilson J. R., Mathews G. J. 1995, *Phys. Rev. Lett.*, 75(23), 4161
- Wilson J. R., Mathews G. J., Marronetti P. 1996, *Phys. Rev. D*, 54, 1317
- Wilson J. R., Mayle R. W. 1993, *Phys. Rep.*, 227, 97
- Yancopoulos S., Hamilton T. T., Helfand D. J. 1994, *ApJ*, 429, 832

A. Appendix: Neutron Star EOS

A key requirement of a gamma-ray burst paradigm based upon collapsing neutron stars in binaries is that the equation of state be relatively soft so that significant compression and heating can occur before inspiral. Therefore, for completeness in this Appendix we review arguments for and against a “soft” neutron star EOS.

The neutron star EOS must extend from normal iron nuclei on the surface to as much as 15 times nuclear matter density in the interior. At the same time, one must consider that neutron stars in weak-interaction equilibrium are highly isospin asymmetric. They may also carry net strangeness. Therefore, only pieces of the neutron-star equation of state, e.g. the nuclear compressibility, are accessible in laboratory experiments. The value for the nuclear compressibility K_s can be derived from the nuclear monopole resonance (Blaizot 1980). The present value ($K_s = 230$ MeV) is consistent with a modestly soft nuclear equation of state.

Nuclear heavy-ion collision data can also be used to shed some insight, particularly for the heated neutron-star equation of state. For example, McAbee & Wilson (1994) studied heavy ion collisions of $^{139}_{57}\text{La}$ on ^{139}La as a means to constrain the supernova EOS. The electron fraction for $^{139}_{57}\text{La}$ ($Y_e = 0.41$) overlaps that of supernovae which range from $Y_e = 0.05$ to 0.50. They showed that the pion contribution to the EOS could be constrained by the observed pion multiplicities from central collisions. The formation and evolution of pions was computed in the context of Landau-Migdal theory to model the effective energy and momenta of the pions. A key aspect of hydrodynamic simulations of the heavy-ion data was the determination of the Landau parameter g' . Their determination of the pion contribution to the equation of state implies a relatively soft equation of state after pion condensation such that a maximum neutron-star mass of $M \leq 1.64 M_\odot$ is inferred.

There have been dozens of nuclear equations of state introduced over the years. Summaries of some of them can be found in Schaab & Weigel (1999) and Arnett & Bowers (1977). As far

as the maximum mass of a neutron star is concerned, most theoretical equations of state fall into two groups, those which only describe the mean nuclear field even at high density and those which allow for various condensates, e.g. pions, kaons, hyperons, and even quark-gluon plasma. Table 5 summarizes the basic neutron star properties based upon most available nuclear equations of state (Lattimer 1998).

Equations of state which are based upon the mean nuclear field tend to be “stiff” at high density. Therefore, they reach lower interior densities for the same baryonic mass and tend to allow a higher maximum neutron-star mass $m_{max} \sim 1.8 - 2.2 M_{\odot}$. Such equations of state also tend to become acausal at the high densities associated with the maximum neutron-star mass. On the other hand, the relativistic equations of state are generally causal at high density. They also tend to be somewhat “soft”, therefore allowing a higher central density for a given baryon mass and generally implying a maximum neutron-star mass in the range $m_{max} \sim 1.3 - 1.7 M_{\odot}$. We note, however, that recent 3-body corrections to a relativistic EOS (Akmal et al. 1999) tend to stiffen an otherwise soft relativistic EOS.

For the most part, constraints on the neutron star equation of state must ultimately come from observations of neutron stars themselves. Over the years attempts have been made with limited success to constrain the equation of state based upon the maximum observed rotation frequency (e.g. Friedman et al. 1986) or the thermal response to neutron star glitches (e.g. Page 1998). In recent years, however, new observational constraints on the structure and properties of neutron stars are becoming available (Lattimer 1998). Observations of quasi-periodic oscillations (QPOs) (Strohmayer et al. 1996; Van Der Klis et al. 1996, 1997), pulsar light curves (Yancopoulos et al. 1994; Thorsett & Chakrabarty 1999), and glitches (Link et al. 1999), studies of soft-gamma repeaters (Kouveliotou et al. 1998; Gotthelf et al. 1999); and even the identification of an isolated non-pulsing neutron stars (Walter et al. 1996; Haberl et al. 1997) have all led to the hope that significant constraints on the mass-radius relation and maximum mass of neutron stars may be soon coming.

A.1. Pulsars

Two possible constraints come from measured pulsar systems. The most precisely measured property of any pulsar system is its spin frequency. The frequencies of the fastest pulsars (PSR B1937+21 at 641.9 Hz and B1957+20 at 622.1 Hz) already constrain the equation of state under the assumption that these pulsars are near their maximum spin frequency (Friedman et al. 1986). In particular, the equation of state cannot be too stiff, though maximum masses as large as $3 M_{\odot}$ are still allowed.

A much more stringent constraint may come from the numerous determinations of neutron-star masses in pulsar binaries. There are now about 50 known pulsars in binary systems. Of these 50, approximately 15 of them have significantly constrained masses. These are summarized

in Table 6. The measured masses are all consistent with low neutron-star masses in the range $m \approx 1.35 \pm 0.10 M_{\odot}$ (Thorsett & Chakrabarty 1999). Even though these masses are low, this does not necessarily mean that the maximum neutron-star mass is in this range. If one adopts these masses as approaching the maximum neutron-star mass, then the softer equations of state are preferred. However, this narrow mass range may be the result of the mechanism of neutron-star formation in supernovae and not an indication of the maximum neutron-star mass.

In a recent paper, Link et al. (1999) have proposed that glitches observed in the Vela pulsar and six other pulsars may place some constraint on the nuclear EOS. In particular, if the glitches originate from the liquid of the inner crust, and if the mass of the Vela pulsar is 1.35 consistent with Table 2, then the radius of the Vela pulsar must be $R \gtrsim 8.9$ km. This result is consistent with either a soft or stiff equations of state. A better theoretical determination of the pressure at the crust-core interface might lead to a more stringent constraint.

A.2. QPO's

The identification of kilohertz QPO's with the last stable orbit around a neutron star also could significantly constrain the neutron-star equation of state (e.g. Schaab & Weigel 1999). For example, demanding that the 1.2 kHz QPO from source KS 1731-260 be the last stable orbit requires a neutron-star mass of $1.8 M_{\odot}$. On the other hand, other interpretations are possible for the origin of QPO's. For example, they could be a harmonic of a lower frequency outer orbit, or they might result from effects closer to the neutron-star surface. Among proposals for the source of the QPO phenomenon are: boundary layer oscillations (Collins et al. 1998); radial oscillations and diffusive propagation in the transition region between the neutron star and the last Keplerian orbit (Titarchuk & Osherovich 1999); Lense-Thirring precession for fluid particles near the last stable orbit (Miller et al. 1998; Merloni et al. 1999; Morsink & Stella 1999); and nonequitorial resonant oscillations of magnetic fluid blobs (Vietri & Stella 1998).

A.3. Supernova constraints

The lack of a radio pulsar in SN1987A, along with nucleosynthesis constraints on the observed change of helium abundance with metallicity has led to the suggestion (Brown & Bethe 1994; Bethe & Brown 1995) that the maximum neutron-star mass must be $\lesssim 1.56 M_{\odot}$. In this picture, the development of a kaon condensate tends to greatly soften the EOS after ~ 12 sec. Thus, even though neutrinos were emitted, the core subsequently collapses to a black hole.

One constraint comes from the neutrino signal itself observed to arise from supernova SN1987A. The fact that the neutrinos arrived over an interval of at least twelve seconds implies a significant cooling and neutrino diffusion time from the core. This favors a soft equation of state in which the core is more compact and at higher temperature in the supernova models. For example, the

simulations of Wilson & Mayle (1993) require a maximum neutron-star mass of $\lesssim 1.6 M_{\odot}$.

A.4. Isolated Neutron Star

A most promising constraint on the neutron-star EOS may come from the determination of the radius for the isolated nonpulsing neutron star RX J185635-3754, first detected by ROSAT (Walter et al. 1996). The inferred (redshifted) surface temperature from the X-ray emission is about 35 eV. Atmospheric models of this emission then imply (Lattimer 1998; An et al. 1998; Wang et al. 1999) that for a distance between 31 and 41 pc, a radius between $5.75 < R/\text{km} < 11.4$ and a mass of $1.3 < M < 1.8$, is most consistent with the observed emission. This is suggestive of a soft equation of state. However, this constraint requires that the distance be less than 41 kpc. On the other hand, Wang et al. (1999) find that the cooling properties of the soft X-ray source RX J0720.4-3125 are most consistent with a moderately stiff or stiff EOS provided that the age of this star is less than 10^5 yr. Proper motion studies with HST are currently underway to determine a reliable distance to RX J185635-3754. These studies will provide a key constraint on the nuclear equation of state.

Table 1. Table of the equation of state for a neutron star with critical mass $M_c = 1.575M_\odot$. Values are baryonic density ρ , specific energy ϵ and $\Gamma \equiv 1 + P/\rho\epsilon$ where P is the pressure.

ρ gm/cm $^{-3}$	ϵ ergs/gm	Γ	ρ gm/cm $^{-3}$	ϵ ergs/gm	Γ
1.00×10^9	1.11×10^{18}	1.386	1.46×10^{13}	1.94×10^{19}	1.150
1.46×10^9	1.28×10^{18}	1.380	2.15×10^{13}	2.03×10^{19}	1.108
2.15×10^9	1.47×10^{18}	1.372	3.16×10^{13}	2.09×10^{19}	1.057
3.16×10^9	1.69×10^{18}	1.367	4.64×10^{13}	2.13×10^{19}	1.052
4.64×10^9	1.94×10^{18}	1.363	6.81×10^{13}	2.17×10^{19}	1.061
6.81×10^9	2.22×10^{18}	1.358	1.00×10^{14}	2.23×10^{19}	1.093
1.00×10^{10}	2.54×10^{18}	1.352	1.46×10^{14}	2.36×10^{19}	1.213
1.46×10^{10}	2.90×10^{18}	1.346	2.15×10^{14}	2.68×10^{19}	1.468
2.15×10^{10}	3.30×10^{18}	1.341	3.16×10^{14}	3.39×10^{19}	1.778
3.16×10^{10}	3.75×10^{18}	1.336	4.64×10^{14}	4.75×10^{19}	1.992
4.64×10^{10}	4.26×10^{18}	1.330	6.81×10^{14}	7.09×10^{19}	2.103
6.81×10^{10}	4.82×10^{18}	1.322	1.00×10^{15}	1.09×10^{20}	2.16
1.00×10^{11}	5.44×10^{18}	1.314	1.46×10^{15}	1.69×10^{20}	2.145
1.46×10^{11}	6.13×10^{18}	1.307	2.15×10^{15}	2.58×10^{20}	2.063
2.15×10^{11}	6.88×10^{18}	1.300	3.16×10^{15}	3.87×10^{20}	2.061
3.16×10^{11}	7.71×10^{18}	1.294	4.64×10^{15}	5.81×10^{20}	2.059
4.64×10^{11}	8.62×10^{18}	1.288	6.81×10^{15}	8.67×10^{20}	2.03
6.81×10^{11}	9.61×10^{18}	1.280	1.00×10^{16}	1.28×10^{21}	2.015
1.00×10^{12}	1.06×10^{19}	1.270	1.46×10^{16}	1.88×10^{21}	2.007
1.46×10^{12}	1.17×10^{19}	1.261	2.15×10^{16}	2.76×10^{21}	2.003
2.15×10^{12}	1.29×10^{19}	1.250	3.16×10^{16}	4.05×10^{21}	2.001
3.16×10^{12}	1.41×10^{19}	1.236	4.64×10^{16}	5.94×10^{21}	2.001
4.64×10^{12}	1.54×10^{19}	1.224	6.81×10^{16}	8.71×10^{21}	2
6.81×10^{12}	1.67×10^{19}	1.216	1.00×10^{17}	1.27×10^{22}	2
1.00×10^{13}	1.81×10^{19}	1.211			

Table 2. Central density and released gravitational energy as a function of the binary angular momentum J in geometrized units. This calculation (Mathews & Wilson 2000) is for a neutron star with $M_B = 1.548 M_\odot$, $M_G = 1.39 M_\odot$, and EOS for which $M_c = 1.575 M_\odot$.

J (10 ¹¹ cm ²)	ρ (10 ¹⁵ g cm ⁻³)	E (10 ⁵² erg)
1.65	1.48	4.3
1.80	1.46	2.4
2.0	1.45	1.5
2.2	1.43	1.0
2.4	1.40	0.7
2.6	1.38	0.6
∞	1.34	0

Table 3. Final Lorentz factor of the baryon wind for a range of initial total energies and entropies per baryon.

Energy (ergs)	Entropy per Baryon		
	10 ⁵	10 ⁶	10 ⁷
10 ⁵¹	175	1750	1.6×10^4
10 ⁵²	350	3100	2.9×10^4
10 ⁵³	525	5500	5.3×10^4

Table 4. The t_{90} duration, in seconds, of external shock GRBs corresponding to the fireballs outlined in Table 3. This t_{90} is calculated energy emitted in photons greater than 10 keV.

Energy (ergs)	Entropy per Baryon		
	10 ⁵	10 ⁶	10 ⁷
10 ⁵¹	40.3	0.7	3.7×10^{-3}
10 ⁵²	21.6	7.2	1.6×10^{-3}
10 ⁵³	23.8	0.17	1.8×10^{-3}

Table 5: Neutron star properties from various equations of state

Equation of State	Composition	Maximum Mass (M_{\odot})	R (km)
Mean Nuclear Field	p, n, e^-, μ^-	$\approx 2.0 \pm 0.20$	$\approx 13 \pm 3$
Exotic Particles/ Condensates	$p, n, e^-, \mu^-, \Lambda, \Sigma^{\pm,0}, \Xi^{0,-},$ $\Delta^{\pm,0,++}, K^{\pm,0}, \pi^{\pm,0}$, quarks, etc.	$\approx 1.5 \pm 0.2$	$\approx 9 \pm 1$

Table 6: Summary of masses of observed pulsars in binaries.

Pulsar	Mass (M_{\odot})
<i>Double Neutron Star Systems</i>	
J1518+4904	1.56 $^{+0.13}_{-0.44}$
J1518+4904	1.05 $^{+0.45}_{-0.11}$
B1534+12	1.339 ± 0.0003
B1534+12	1.339 ± 0.0003
B1913+16	1.4411 ± 0.00035
B1913+16	1.3874 ± 0.00035
B2127+11C	1.349 ± 0.040
B2127+11C	1.363 ± 0.040
B2303+46	1.30 $^{+0.13}_{-0.46}$
B2303+46	1.34 $^{+0.47}_{-0.13}$
<i>Neutron Star/White-Dwarf Systems</i>	
J1012+5307	1.7 ± 0.5
J1713+0747	1.45 ± 0.31
J1713+0747	1.34 ± 0.20
B1802-07	1.26 $^{+0.08}_{-0.17}$
B1855+09	1.41 ± 0.10
<i>Neutron Star/Main-Sequence Systems</i>	
J0045-7319	1.58 ± 0.34